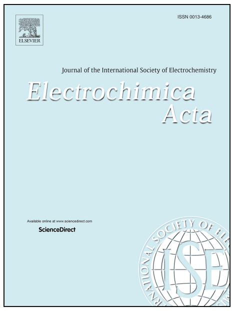

Facile synthesis of CoSe nanoparticles encapsulated in N-doped carbon nanotubes-grafted N-doped carbon nanosheets for water splitting

Ming Yang, Yuanyuan Yang, Kaizhi Wang, Shuwen Li, Fan Feng, Kai Lan, Pengbo Jiang, Xiaokang Huang, Honglei Yang, Rong Li

PII: S0013-4686(20)30076-1

DOI: https://doi.org/10.1016/j.electacta.2020.135685

Reference: EA 135685

To appear in: *Electrochimica Acta*

Received Date: 14 March 2019

Revised Date: 18 December 2019

Accepted Date: 9 January 2020

Please cite this article as: M. Yang, Y. Yang, K. Wang, S. Li, F. Feng, K. Lan, P. Jiang, X. Huang, H. Yang, R. Li, Facile synthesis of CoSe nanoparticles encapsulated in N-doped carbon nanotubes-grafted N-doped carbon nanosheets for water splitting, *Electrochimica Acta* (2020), doi: https://doi.org/10.1016/j.electacta.2020.135685.

Facile synthesis of CoSe nanoparticles encapsulated in N-doped carbon nanotubes-grafted N-doped carbon nanosheets for water splitting

*Ming Yang, Yuanyuan Yang, Kaizhi Wang, Shuwen Li, Fan Feng, Kai Lan, Pengbo Jiang, Xiaokang Huang, Honglei Yang and Rong Li **

State Key Laboratory of Applied Organic Chemistry (SKLAOC), The Key Laboratory of Catalytic Engineering of Gansu Province, College of Chemistry and Chemical Engineering, Lanzhou University, Lanzhou, 730000, P. R. China. E-mail: liyirong@lzu.edu.cn; Fax: +86-931-891-2582; Tel: +86-18919803060.

ABSTRACT

Rationally designing a high-efficiency, inexpensive and stable electrocatalyst is important in the renewable energy field. Herein, a one-step strategy is adopted to synthesize 3D hybrid of CoSe nanoparticles encapsulated nitrogen-doped carbon nanotubes graft onto nitrogen-doped carbon nanosheets (denoted as CoSe@NCNT/NCN) with excellent hydrogen evolution reaction (HER) and oxygen evolution reaction (OER) activity in acidic and alkaline solutions, respectively. Benefiting from the unique morphology, the large surface area and good conductivity, the hybrid exhibits excellent electrocatalytic HER activity in 0.5 M H_2SO_4 solution, which is a low overpotential of 197 mV at a current density of 10 mA cm^{-2} with a Tafel slope of 43 mV dec^{-1}. Meanwhile, it presents a low overpotential of 301 mV at a current density of 10 mA cm^{-2} with a Tafel slope of 75 mV dec^{-1} in 1 M KOH solution for OER. The good electrocatalytic property is comparable to most of the previously reported Co-based electrocatalysts and the synthetic method is low toxic and simple, which may be expanded to other transitional metal dichalcogenides. The strategy provides a possibility for preparation for effective nonprecious high performance HER and/or OER electrocatalysts.

KEYWORDS

Hydrogen evolution reaction, Oxygen evolution reaction, water splitting, N-doped carbon nanotubes, CoSe nanoparticles.

1. Introduction

The importance of dealing with the global energy crisis and developing a low-carbon energy resource has given the motivation to research sustainable clean energy.[1] Recently, the study of electrochemical water splitting has triggered attention in that it can provide an environmentally-friendly hydrogen production technology and make full use of other energy (solar and wind energy).[2-4] There are two half reactions during the process of water splitting: hydrogen evolution reaction (HER) at cathode and oxygen evolution reaction (OER) at anode. However, the sluggish kinetics of OER has limited the entire electrolytic process.[5] To date, precious metals are still the best catalysts in water splitting. But the scarcity and expensiveness limit the applications in the commerce. In the past decades, nonprecious metal catalysts (transition metal phosphides,[6-8] sulfides,[9, 10] selenides,[11-13] borides[14-17] and carbides[18, 19]) grew in various nitrogen-containing carbon supports and metal-free catalysts[20, 21] have been studied, which possessed excellent activity and stability for HER and/or OER.

Cobalt selenide as a representative highly active transition metal dichalcogenide and earth-abundant catalyst is an alternative to novel metal catalysts, and it has recently been researched extensively due to its high electrochemical stability, inexpensiveness and environmental friendliness.[22-24] Many reported cobalt selenide catalysts for water electrolysis are primarily $CoSe_2$-based electrocatalysts, however, few investigations have been done on CoSe as electrocatalysts. The CoSe catalyst has also higher electrochemical activity, which is mainly attributed to moderate bond between Se/Co species.[25] In order to further enhance their electrochemical catalytic property and the stability in corrosive environment, a nitrogen-doped carbon material was utilized as a supporter, which could not only prevents the agglomeration of the nanoparticles but also slows down the corrosive speed of catalysts.[26] In addition, the doped nitrogen functioned as active sites because it could modulate charge distribution for the HER and OER. Recently, the integration of 1D nitrogen-doped carbon nanotubes (NCNTs) and 2D carbon nanosheets into 3D hierarchical carbon hybrid have triggered attention because they can protect the metals/metal compounds in corrosive solution and afford an excellent conductive carrier for electronic transfer. For instance, Chen et al. developed Co nanoparticles embedded in NCNTs-grafted graphene sheets for HER;[27] Zhou et al. designed $CoSe_2$ nanoparticle embedded in carbon nanotube as effective HER electrocatalyst;[28] Guo et al. devised Co_2P-CoN confined in N-doped carbon nanotube for HER, OER and ORR.[29] Nonetheless, the fabrication process of these catalysts is still complex and multi-step. Hence, it is vital to develop a facile and economic way to fabricate a transition metal dichalcogenide, which is encapsulated in nitrogen-doped carbon nanotubes.

Herein, we rationally design a 3D hierarchical N-doped carbon hybrid in which CoSe nanoparticle was encapsulated within nitrogen-doped carbon nanotube (NCNT) graft onto nitrogen-doped carbon nanosheet (NCN) (CoSe@NCNT/NCN) by a facile one-step carbonization-selenylation process using cobalt acetate, selenium powder, melamine and glucose as precursors under a H_2/Ar atmosphere. The as-synthesized catalyst was applied as an effective electrocatalyst for HER in acidic and OER in basic solutions, exhibiting outstanding electrochemical performance with the overpotential of 197 mV and 301 mV at current density of 10 mA cm^{-2} in acidic and basic solutions, respectively. The excellent electrocatalytic effect was mainly due to the unique morphology, the lager active surface area and the synergistic effects between CoSe nanoparticles and 3D conductive N-doped carbon networks.

2. Experimental Section

2.1. Materials

Cobalt (□) acetate tetrahydrate ($Co(CH_3COO)_2 \cdot 4H_2O$), selenium powder, melamine ($C_3H_6N_6$), glucose and ethanol were purchased from Sinopharm Chemical Reagents Beijing Co. Lid. Nafion (0.5 wt%), commercial Pt/C catalyst and iridium (IV) oxide were purchased from Alfa Aesar. DI water (18.2 MΩ cm) was added during the entire process of experiment. All reagents were applied directly without further purification.

2.2. Preparation of CoSe@NCNT/NCN

The catalyst was obtained through two-step heat up carbonization. In a typical method, melamine (3 g), glucose (100 mg), cobalt acetate tetrahydrate (500 mg) and excess selenium powder were dissolved in a mixture of 50ml ethanol and DI water (1:1). The solution was continuously stirred until a homogeneous suspension, which was totally dried to solid. The solid was finely grinded using a mortar and pestle. The resulting precursor was sent to a porcelain boat and was heated at 600 ^{o}C for 2h and was further heated up to 900 ^{o}C and lasted for another 2h, during which the speed of heating was 2 ^{o}C per minute. The whole process was protected under a mixture of Ar/H_2 (5 %). The collected product was recorded as CoSe@NCNT/NCN. In addition, some other samples were fabricated by changing the heating temperature during the second step from 600 ^{o}C to 800 ^{o}C and 1000 ^{o}C not altering the other parameters. The obtained samples were named after CoSe@NCNT/NCN-X (where X refers to the temperature). The different level of CoSe amounts were performed by altering the content of cobalt acetate tetrahydrate and selenium powder in precursor.

2.3. Preparation of Co@NCNT/NCN

Co@NCNT/NCN was obtained by the same procedure without adding selenium powder at 900 ^{o}C.

2.4. Preparation of bulk CoSe and NCN

The bulk CoSe was gotten with a mixture of cobalt acetate tetrahydrate and selenium powder pyrolysis at 800 ^{o}C at a heating speed of 5 $^{o}C\ min^{-1}$ under Ar/H_2 (5 %) protection. The nitrogen-doped carbon nanosheets were acquired with a mixture of melamine (3 g) and glucose (100 mg) heated at 600 ^{o}C for 2h and was further heated up to 900 ^{o}C lasting for another 2h with a heating rate of 2 ^{o}C min^{-1} under Ar/H_2 (5 %) protection.

2.5. Electrode preparation and electrochemical measurements

By ultrasound, 5 mg as-synthesized catalyst powder was homogeneously dispersed in a mixture of 470 µL ethanol, 500 µL DI water and 30 µL Nafion solution (0.5 wt%) to obtain a ink. And then, 5µL obtained catalyst ink was dropped on a glass carbon electrode (GCE, diameter: 3 mm), in which the capacity of loading was 0.357 mg cm^{-2}. The electrochemical measurements were operated with a three-electrode electrochemical workstation (CHI660E Shanghai Chenhua Equipment, China) under room temperature. A graphite rod is treated as counter electrode and an Ag/AgCl (3.0 M KCl) as reference electrode in 0.5 M H_2SO_4 and 1.0 M KOH solution, respectively. Each of corresponding current density was standardized by the consistent geometrical zone of the GCE (0.07 cm^2).

3. Results and discussion

A facile one-pot pyrolysis to synthesize N-doped CoSe nanoparticles encapsulated CNTs grafted onto NCN from melamine, glucose, cobalt acetate and selenium powder was illustrated in Scheme 1. A possible growth mechanism was presented: firstly, cobalt acetate was dissociated to cobalt oxide and gaseous species and then selenium powder and cobalt oxide underwent a reaction to yield cobalt selenide nanoparticles, meanwhile, melamine began to undergo thermal decomposition to produce graphic carbon nitride (g-C_3N_4).[30, 31] During heating the mixtures under a protective flow of Ar/H_2 (5 %), the temporary sandwich-like template (graphic carbon nitride and carbon nanosheets) formed at about 600 ^{o}C, which g-C_3N_4 was as a sacrificial template and the stacking thickness of the template was adjusted by changing the quantity of glucose and melamine.[32] Secondly, when the temperature was higher than 700 ^{o}C, the g-C_3N_4 template was completely disintegrated to nitrogen and cyano fragments.[33] Under the catalysis of CoSe, the N-doped CNTs were grown gradually assembling on preformed CoSe nanoparticle (Figure S1c-h and Figure S2c-f) via a tip-growth mechanism[34, 35] to yield the final N-doped

CoSe nanoparticles encapsulated CNTs grafted onto NCNs.

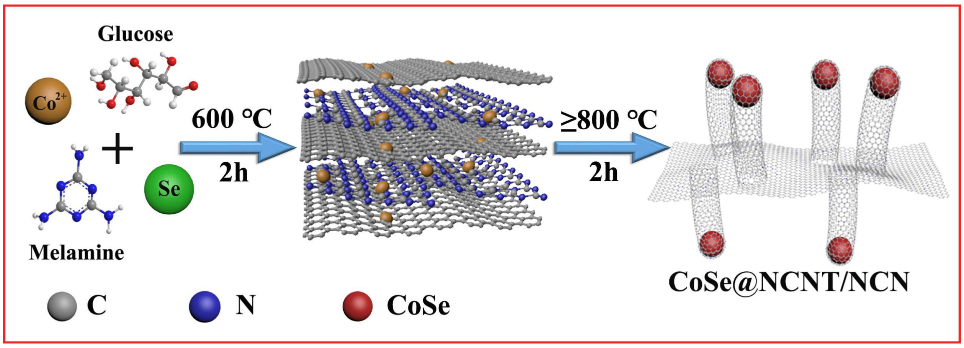

Scheme 1. Schematic illustration of the synthesis procedure of CoSe@NCNT/NCN

The SEM images (Figure 1a-b) show the morphology and microstructure of the CoSe@NCNT/NCN. As depicted in Figure S1, the NCN exhibits a crumpled and layered construction (Figure S1a and Figure S2a), the CoSe nanoparticles were loaded on carbon nitride at 700 °C, until the temperature was above 800 °C, the unique 3D hierarchical structure didn't gradually form (Figure S1c-h). From high magnified SEM images (Figure 1b), the CoSe nanoparticles were discovered within the tip of NCNTs, further verifying the tip-growth mechanism. TEM images further demonstrate CoSe nanoparticles were encapsulated in NCNTs (Figure 1c), and the drop-shaped CoSe particles were observed in the top of the NCNTs, meanwhile, the NCNs were observed around NCNTs (Figure S2c-f). The carbon layers not only prevent the agglomeration and corrosion of CoSe nanoparticles, but also enhance their conductivity and catalytic activity.[36] The high resolution transmission electron microscopy (HRTEM) image (inset of Figure 1c) reveals the clear lattice fringes of CoSe nanocrystal, which can be seen with a lattice distance of 0.313 nm related to the (100) plane, indicating the high degree of crystallinity. The TEM elemental maps (Figure 1e-h) of the summit of NCNTs verify the presence of Co, Se, C and N, which is consistent with XPS analysis results (Figure 3 and Table S3). Clearly, the mapping of N element suggests the N uniformly disperses on carbon nanotubes and the independent mappings of Co and Se indicate the drop-shaped CoSe particle was synthesized successfully.

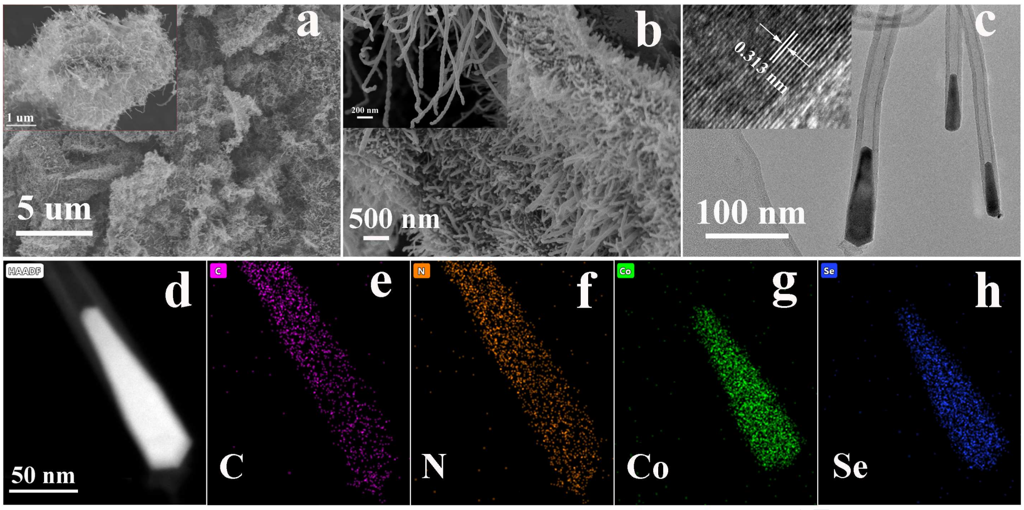

Figure 1. (a, b) SEM images of CoSe@NCNT/NCN and (c) TEM and HRTEM (inset) image, (d) HAADF-STEM and (e-h) element mapping images of CoSe@NCNT/NCN.

The synthesis procedure can be also revealed by X-ray powder diffracting (XRD) patterns of CoSe@NCNT/NCN during the pyrolysis process as shown in Figure 2a-b, and the XRD pattern illustrates the existence of $CoSe_2$ (JCPDS No.65-3327) at 600 ^{o}C. When the temperature further rises to 700 ^{o}C, the peaks of $CoSe_2$ convert to that of CoSe (JCPDS No.89-2004), which means $CoSe_2$ is reduced to CoSe because of the existence of abundant carbon resource, and this result is consistent with the HRTEM consequence above. From 700 to 900 ^{o}C, the CoSe isn’t reduced until 1000 ^{o}C, at which it is partly reduced to Co (JCPDS No.89-7093). The hybrid has the highest electrochemical catalytic activity and the lowest overpotential when it is heated to 900 ^{o}C for 2 h. And this result is in accordance with previous reports,[34, 37] which reveals that the activity of catalysts is influenced by the heating temperature. To demonstrate the important element Se, the Co nanoparticles encapsulated N-doped CNTs grafted onto NCN (Co@NCNT/NCN) was synthesized by the same procedure without adding selenium powder. From Figure 2a, the XRD pattern exhibits that Co exists in N-doped carbon hybrid. The samples with different level of CoSe amounts were prepared by controlling Co^{2+} and selenium content. From Figure S3, the SEM images show that CoSe/NCNT@NCN was also well synthesized as we reduced the Co^{2+}

content from 2 mmol to 1 mmol (Figure S3a-b). When the content of Co^{2+} increased to 3 mmol, more unencapsulated CoSe particles loaded on the surface of the carrier are revealed in Figure S3c-d clearly, because the relative amount of melamine decreased and that of cobalt increased. The results indicate that controlling the ratio of Co to melamine in a certain range is the key to the effective synthesis of the catalyst. To further research the defects information of as-synthesized carbon materials, the Raman spectra of the four different annealed catalysts are shown in Figure S4, in which the D-band at around 1335 cm^{-1} represents the disorder carbon while G-band at around 1586 cm^{-1} illustrates the graphitic carbon. The D to G-band (I_D/I_G) intensity ratio indicates that the rise of pyrolysis temperature leads to higher graphitization degree of CoSe@NCNT/NCN and lower content of nitrogen that in accordance with CHN elemental analysis (Table S4). So the appropriately improved temperature to keep a balance (900 ^oC) is beneficial to catalytic activity and conductivity. The superficial area and pore distribution of as-synthesized sample are analyzed using nitrogen adsorption-desorption isotherm. As shown in Figure 2c, CoSe@NCNT/NCN presents a typical IV-type isotherm with a typical H3 hysteresis loop at a relative pressures (0.4–1P/P_0), suggesting the mesoporous characteristic of catalyst. The specific surface area of the catalyst is measured by Brunauer-Emmet-Teller (BET) method, which possesses a high specific surface area of 153.5 m^2 g^{-1} with a Pore Volume of 0.33 cm^3 g^{-1}. High surface areas and mesoporous architecture could amplify the electrochemical active surface area of electrocatalysts and accelerate the reactants and products transport rate,[38] resulting in higher electrochemical activity. The thermogravimetric analysis (TGA) of CoSe@NCNT/NCN (Figure 2d) suggests that the content of CoSe is about 38 %.

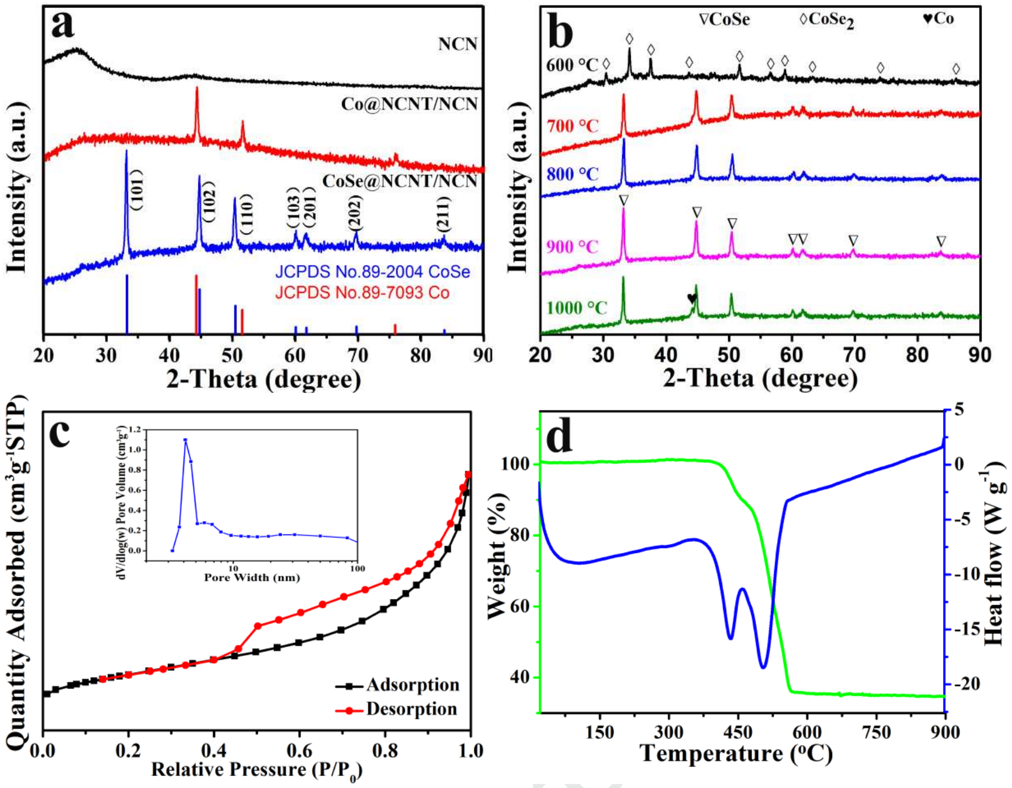

Figure 2. (a) XRD patterns of NCN, Co@NCNT/NCN and CoSe@NCNT/NCN, (b) XRD patterns of CoSe@NCNT/NCN at different temperature, (c) N_2 adsorption–desorption isotherms and the pore size distribution plot (inset) of Co@NCNT/NCN, (d) TGA and DSC curves of CoSe@NCNT/NCN

To further clarify the chemical constituents and states of the CoSe@NCNT/NCN, X-ray photoelectron spectroscopy (XPS) measurements were operated. Figure S5 shows the full-scan XPS spectra, the CoSe@NCNT/NCN surface mainly detects the signals of C, N, Co, Se and O elements. When the temperature changes from 800 to 1000 ^{o}C, the N 1s peak weakens suggesting the content of N reduce with the rise of temperature which is in accordance with previous research[39]. The existence of the oxygen signal is possibly because the adsorbed oxygen-species by contacting with air. The electrocatalysts atomic content was analyzed by XPS data (Table S3), the content of C in the XPS data is much more than that in CHN elemental analysis, which is a pretty good proof that the CoSe nanoparticles were encapsulated in CNTs, because the detective distance of XPS measurement is only about 2.0 nm.[40, 41] High resolution XPS spectra of Co $2p_{1/2}$ and Co $2p_{3/2}$ (Figure 3c) can be deconvoluted into Co^0, Co^{2+} and satellite peaks, respectively. The peaks located at 778.4 and 794.0 eV are assigned to reduced Co species, the peaks at 780.8 and 796.9 eV reflect the existence of Co^{2+}, which are accordance with Co species in CoSe, and the peaks at 785.0 and 803.1 eV are attributed to shake-up satellite peaks of Co 2p, indicating the antibonding orbital between the Co and Se atom.[42, 43] Figure 3d shows the spectrum of Se 3d, the peaks at 55.1 and 54.2 eV are owing to Se $3d_{3/2}$ and Se $3d_{5/2}$, respectively, which is also in conformance to Co-Se of CoSe. The additional peak at 59.4 eV is ascribed to the surface SeO_x, and the another peak at 60.9 eV is ascribed to Co 3p, consistent with the reported articles.[44] As shown in Figure 3a, the high resolution C 1s XPS spectrum is fitted into three bonds located at 284.7, 285.3 and 286.3 eV, which is due to C-C, C-N, and C-O bonds, respectively.[45, 46]The C-N bond indicates the existence of doping N. Furthermore, the high resolution XPS spectrum of N 1s (Figure 2b) is fitted to four peaks with binding energy at 399.0, 398.4, 401.2, and 406.9 eV, for the pyrrolic N, pyridinic N, graphitic N and oxygenated N, respectively. From Figure S8, the percentage of pyridinic N reduced markedly and the graphitic N increased notably with the rise of heating temperature, which is accordance with previous research.[37, 47] Therefore, the content of N decreased to appropriate level is good for improving the conductivity and the activity of catalysts.

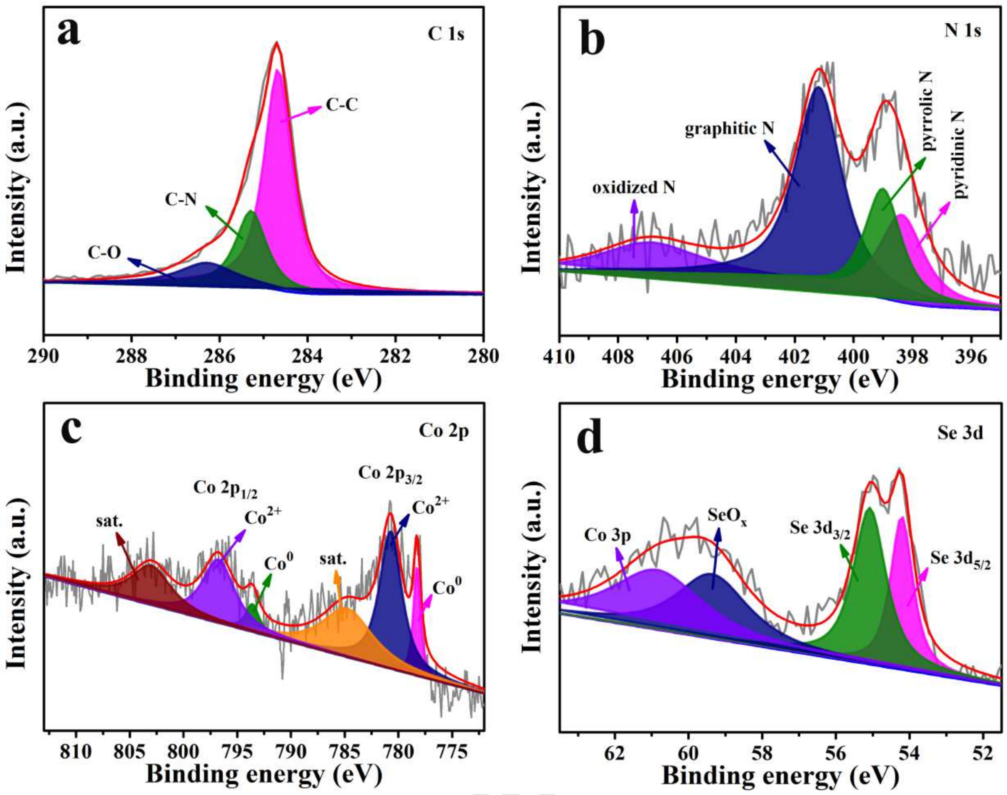

Figure 3. The high resolution spectra (a) C 1s (b) N 1s (c) Co 2p (d) Se 3d of CoSe@NCNT/NCN

The hierarchical 3D architecture of the as-prepared CoSe@NCNT/NCN presents excellent electrochemical performance, which is better than other samples. The HER and OER performance of all catalysts are assessed in N_2-saturated 0.5 M H_2SO_4 solution and O_2-saturated 1 M KOH solution, respectively, and the scan rate is 5 mV s^{-1} with a same loading of approximately 0.357 mg cm^{-2} at room temperature.

The HER polarization curves acquired by linear sweep voltammetry (LSV) are showed in Figure 4a and b. CoSe@NCNT/NCN shows more excellent electrocatalysis activity than others, possessing the lowest overpotential η=-197 mV at 10 mA cm^{-2} (a metric concerned solar fuel synthesis), which is smaller than CoSe@NCNT/NCN-800 (η=-202 mV) and CoSe@NCNT/NCN-1000 (η=-247 mV). The HER performance of the CoSe@NCNT/NCN could mainly ascribe to the charged Se and Co species, as an excellent electrocatalyst should have weaker hydrogen bonds duly releasing the generated product. Se and Co are principally active sites acting as proton-acceptor and hydride-acceptor centers for HER, respectively. The isolated metal center with a positive charge as hydride-acceptor sites weakens the selenium-hydrogen bonds and reduces the energy barrier of the formation of hydrogen-hydrogen bonds.[48] Meanwhile, the NCNTs combined with NCNs could promote the transfer of reactants and products and expose more active catalysis sites for HER. In addition, the synergistic effect of pyrrolic N and CoSe related to improves the HER activity, because that previous studies have shown that lone pair electrons in pyrrolic N are considered catalytic centers.

The underlying mechanism of HER is revealed via Tafel plots derived from the LSV curves. In general, there are three theoretical reaction mechanisms of HER in acidic media.[49] Firstly, the Volmer reaction (theoretical Tafel slope of 118.2 mV dec^{-1}) is primary discharge step, in which the adsorption of hydrogen on the catalyst active sites switches to intermediate state hydrogen. Secondly, the Heyrovsky reaction (theoretical Tafel slope of 39.4 mV dec^{-1}) is the step of electrochemical desorption and the Tafel reaction (theoretical Tafel slope of 29.6 mV dec^{-1}) is recombination step. As shown in Figure 4c, the Tafel slope of CoSe@NCNT/NCN (43mV dec^{-1}) is smaller than that of Co@NCNT/NCN (66 mV dec^{-1}), bulk CoSe (92 mV dec^{-1}) and NCN (159 mV dec^{-1}), indicating CoSe and N-doped carbon network have a synergistic effect to obtain superior catalytic performance. The small Tafel slope of as-prepared catalyst is 43 mV dec^{-1}, implying the Volmer-Heyrovsky is the catalytic mechanism for HER and the desorption of hydrogen is the rate-limiting step.

To further understand the catalytic activity of CoSe@NCNT/NCN electrode, the electrode kinetics is examined by electrochemical impedance spectroscopy (EIS). The smaller semicircular (represents charge-transfer resistance R_{ct}) is beneficial to the electrochemical kinetics between the interface of electrolyte and electrocatalyst, indicating faster charge transfer speed. As shown in Figure S10f, we found that CoSe@NCNT/NCN electrode owned a smallest R_{ct} than other catalysts, suggesting fast electron transfer speed on the interface between electrode and electrolyte and good electrical conductivity. In addition, the larger electrochemical surface area (ECSA) represents more electrochemical active sites for catalysts. Therefore, the C_{dl} (double-layer capacitance) of the catalysts were obtained firstly and shown in Figure 4e. The C_{dl} is calculated via utilizing CV measurements in a non-faradic region with the potential range of 0.10-0.20 V vs. RHE at different scan rates from 20 to 180 mV s^{-1} (Figure S10a-e). The C_{dl} of CoSe@NCNT/NCN is calculated to be 4.70 mF cm^{-2}, which is larger than that of CoSe@NCNT/NCN-800 (4.51 mF cm^{-2}), CoSe@NCNT/NCN-1000 (3.04 mF cm^{-2}), Co@NCNT/NCN (1.79 mF cm^{-2}) and bulk CoSe (0.22 mF cm^{-2}), indicating it has more active sites for catalysis. The specific ECSA values of all catalysts were shown in Table S1, in which the CoSe@NCNT/NCN-900 exhibits the largest ECSA in consistent with the electrocatalytic performance for HER. Furthermore, to further investigate the intrinsic HER activity, the turnover frequency (TOF) values for samples were calculated and listed in Table S2. The TOF value of CoSe@NCNT/NCN-900 is 0.1519 s^{-1} at the overpotential of 220 mV, which is higher than that of other samples. The result of TOF values show that CoSe@NCNT/NCN-900 owns more active sites in per cm^2 and higher atomic utilization. The conclusion is consistent with the result of the optimum pyrolysis temperature at 900 °C.

In addition to the activity, the high stability is essential for a electrocatalyst to be used in water splitting. The CoSe@NCNT/NCN maintains the previous LSV curve with slight decay of the cathodic current after 2000 cycles of CV (Figure 4f). And after continuous 18h operation it still shows long time durability in acidic solution.

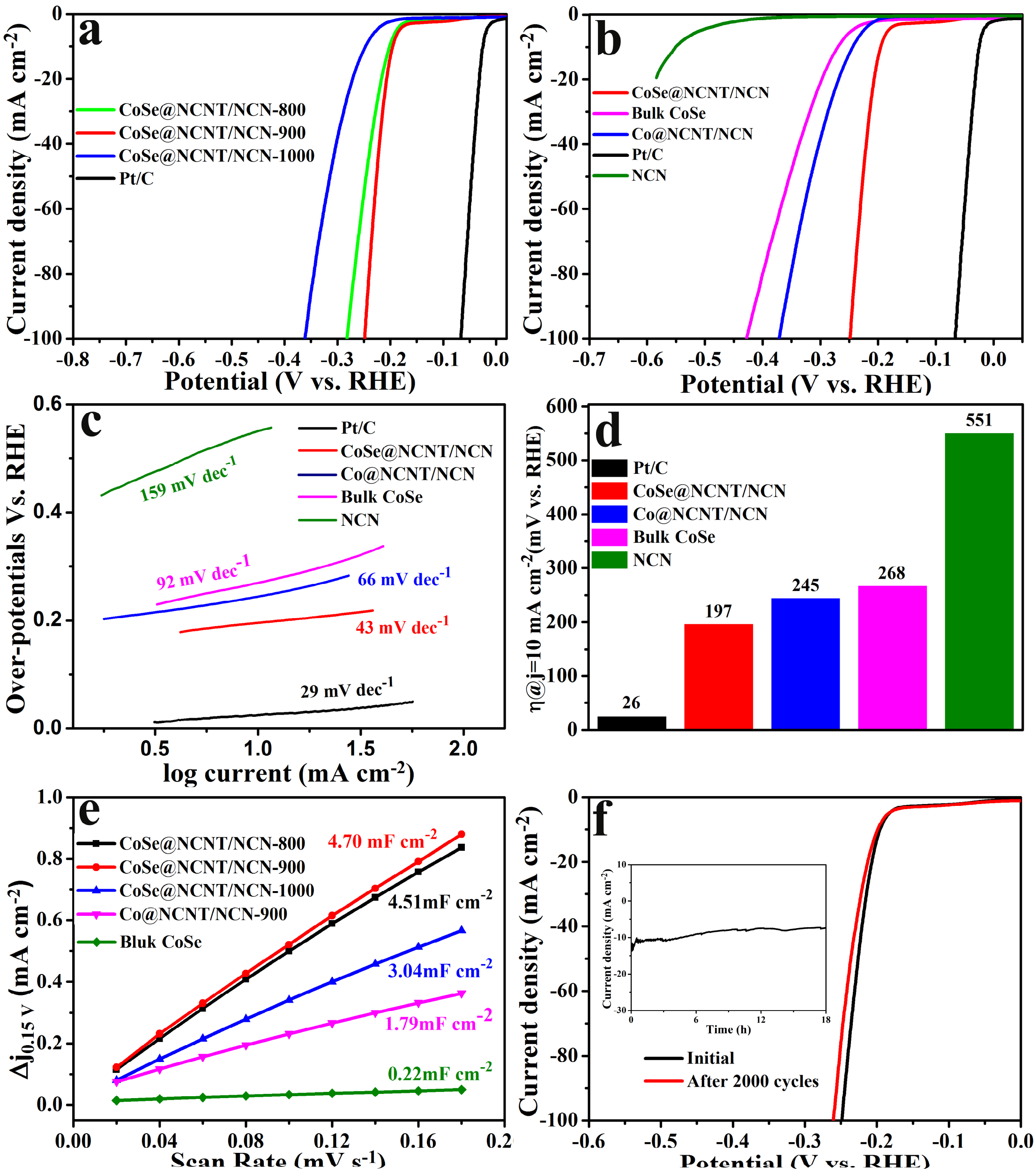

Figure 4. (a) LSV curves of CoSe@NCNT/NCN at different temperature and (b) CoSe@NCNT/NCN, Co@NCNT/NCN, bulk CoSe, NCN and Pt/C in N_2-saturated 0.5 M H_2SO_4 (sweep rate of 5 mV s^{-1}), (c) the corresponding Tafel slopes and (d) the overpotentials at 10 mA cm^{-2}, (e) capacitive current densities of the catalysts with different scan rates, (f) LSV curves of CoSe@NCNT/NCN after 2000 cycles (inset: i-t curve of 18 h).

The OER is a 4-electron transfer process with sluggish kinetics. And sluggish kinetics limits the entire process of water electrolysis, which has been proved by theories.[50] The electrochemical OER tests of

CoSe@NCNT/NCN are evaluated by the LSV curves in O_2-saturate 1.0 M KOH solution at a scan speed of 5 mV s^{-1} using a three-electrode configuration. As shown in Figure 5a and b, the activity of CoSe@NCNT/NCN is evidently better than that of other samples, and it displays a lowest overpotential of η=301 mV at 10 mA cm^{-2}. The overpotential of CoSe@NCNT/NCN is smaller than that of Co@NCNT/NCN (340 mV) and bulk CoSe (380 mV). It is nearly close to commercial IrO_2 catalyst (304 mV) and some of recently reported OER catalysts (Table S6), which means the synthesized catalyst clearly showing a superior electrocatalysis performance. Meanwhile, the Co-Se bond endows the Co element a higher valence state and the NCNTs combined with NCN promote the transfer of reactants and products. They expose more catalysis active sites for OER.[51]

The Tafel slope of CoSe@NCNT/NCN (75 mV dec^{-1}), Co@NCNT/NCN (69 mV dec^{-1}), bulk CoSe (86 mV dec^{-1}), NCN (365 mV dec^{-1}) and the commercial IrO_2 (63 mV dec^{-1}) are displayed in Figure 5c. The NCN shows very high overpotential and Tafel slope, but pure CoSe possesses low overpotential and Tafel slope, indicating that the catalytic activity sites are from CoSe mainly. In contrast, CoSe@NCNT/NCN exhibits superior electrocatalytic properties better than other recently reported nonprecious-metal OER catalysts. The excellent OER property of synthesis catalyst primarily ascribes to the synergistic effect of CoSe particles and N-doped carbon material. The in situ growth NCNTs make the electrochemical active sites of Co more electrophilic by influencing electron density of Co atoms to enhance the adsorption of OH^- groups with CoSe@NCNT/NCN resulting in excellent OER performance. Besides, the carbon nanotubes can offer ordered channels for charge transfer and the 3D hierarchical structure enhances the conductivity and specific surface area of the CoSe@NCNT/NCN catalyst, thus resulting in improved OER activity and stability. Moreover, the synthesis catalyst has a smaller semicircular diameter in EIS than Co@NCNT/NCN and bulk CoSe (Figure S11f), revealing its small electrochemical impedance and fast charge transport between electrocatalyst and electrolyte interface. The content of nitrogen can be determined by CHN elemental analysis, the high N content can act as OER active sites and is beneficial to incorporation metal species, but improving graphitization degree should be beneficial to electrical conductivity with decreasing the content of N, so the temperature of 900 ^{o}C is the better balance.

The unique morphology of the CoSe@NCNT/NCN not only provides shorter diffusion path for electron transfer but also affords a large specific surface area to increase catalytic activity sites, which have been calculated with the electrochemical surface area (ECSA) by measuring the C_{dl} in non-Faradic reaction region (1.20-1.30 V vs. RHE) at different scan rates from 20 to 180 mV s^{-1} (Figure S9a-e). As shown in Figure 5e, the obtained C_{dl} of CoSe@NCNT/NCN is (6.88 mF cm^{-2}), higher than that of CoSe@NCNT/NCN-800 (6.75 mF cm^{-2}), CoSe@NCNT/NCN-1000 (4.25 mF cm^{-2}), Co@NCNT/NCN (3.19 mF cm^{-2}) and bulk CoSe (0.46 mF cm^{-2}). The ECSA value of sample is calculated using the corresponding C_{dl}. From Table S1, the CoSe@NCNT/NCN-900 catalyst has the largest ECSA, which means exposing more active sites than other catalysts amplifying the soild-liquid interface contact of electrolyte and catalytic. Similarly, the CoSe@NCNT/NCN-900 exhibits the highest TOF value of 0.048s^{-1} among the other samples, indicating a effective atomic utilization in OER.

In addition to the outstanding catalytic activity, long-term durability of the electrocatalysis represents another critical parameter for OER. Figure 5f show the CoSe@NCNT/NCN retains the analogous LSV curve after continuous 2000 cycles. The i-t curve is displayed in the inset of Figure 5f, indicating the CoSe@NCNT/NCN possesses the long-term durability in 1 M KOH solution in the 20 h continuous testing.

Furthermore, the XRD, TEM and EDX characterization were used to further investigate the catalyst phase, morphology and compositions of CoSe@NCNT/NCN after long-term test in acidic for HER and in basic for OER. As shown in Figure S12, the XRD pattern of the post-HER CoSe@NCNT/NCN shows pure CoSe phase, illustrating it good stability for HER in acidic media. But the XRD pattern of the post-OER sample exhibits the degradation of the CoSe phase, because small amount of metal oxide is formed. The TEM images in Figure S13a-b exhibit that the morphology of the sample was well preserved in acidic solution, with N-doped CNTs grafted on

NCNs. The CoSe nanoparticle encapsulated N-doped CNTs most were not damaged in Figure S13c-d, which means the morphology was well retained. The surface element distribution of catalyst after durability test was obtained by EDX. From Figure S14-15, the relative oxygen content of the post-OER catalyst was significantly higher than that of the post-HER sample. The result is in good agreement with the XRD, which is mainly due to partly oxidized CoSe phase under OER process.

Finally, we expected that the CoSe@NCNT/NCN was used for overall water splitting. Therefore, a two-electrode cell has been set up in 1.0 M KOH using CoSe@NCNT/NCN-900 as both the anode and cathode (dropped onto carbon paper 0.4 mg/cm^2). As shown in Figure S16, the sample exhibits large implemented potential of 1.82 V at 10 mA cm^{-2}. Apparently, the electrochemical performance of CoSe@NCNT/NCN-900 for overall water splitting is inferior to that of catalysts reported previously, mainly due to the poor HER activity of CoSe in alkaline medium because the mechanism of HER is different in alkaline and acidic solutions. However, the sample exhibits better HER and OER activity in 0.5 M H_2SO_4 and 1.0 M KOH, respectively.

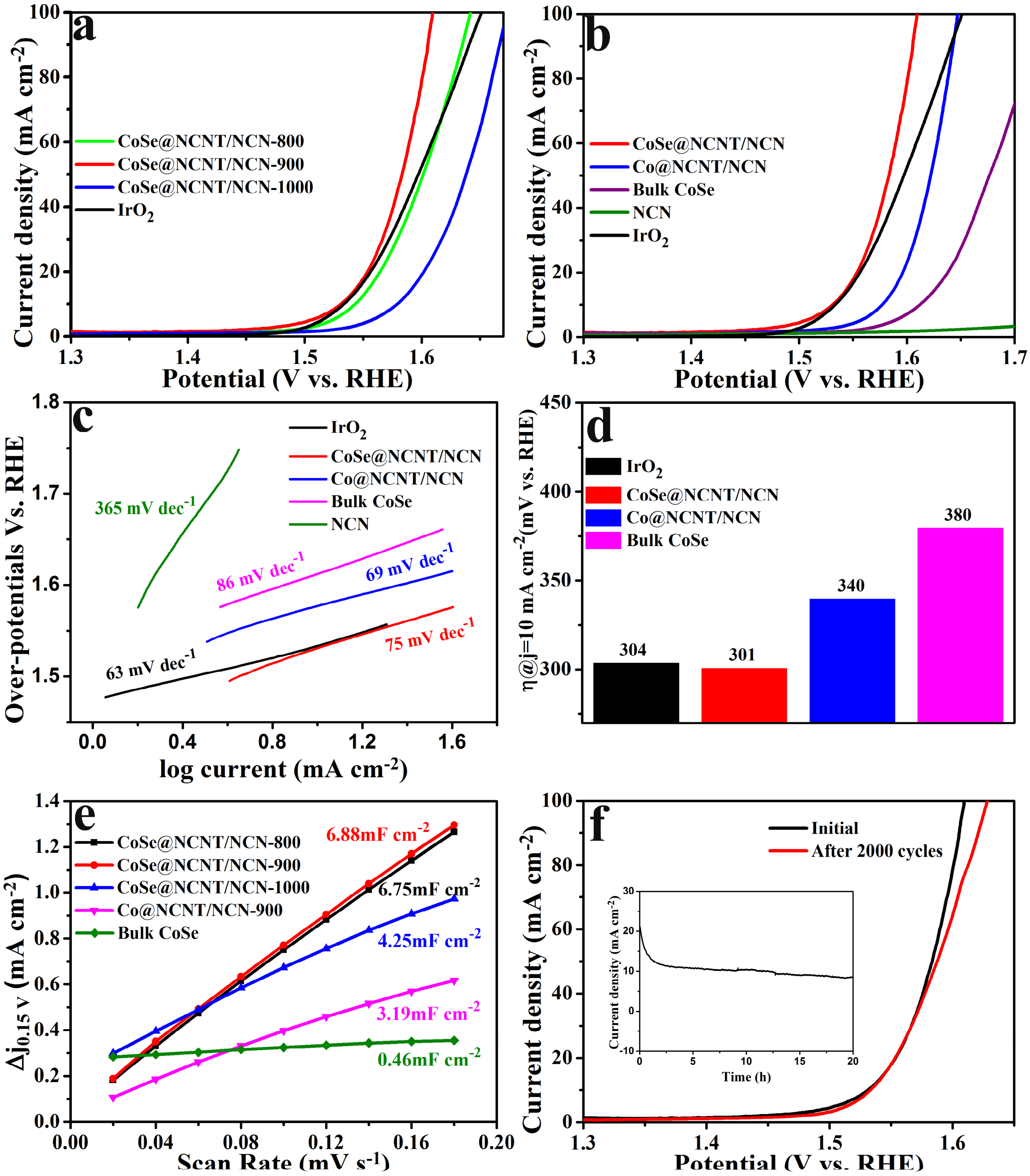

Figure 5. (a) LSV curves of CoSe@NCNT/NCN at different temperature and (b) CoSe@NCNT/NCN, Co@NCNT/NCN, bulk CoSe, NCN and IrO_2 in O_2-saturated 1 M KOH (sweep rate of 5 mV s^{-1}), (c) the corresponding Tafel slopes and (d) the overpotentials at 10 mA cm^{-2}, (e) capacitive current densities of the catalysts with different scan rates, (f) LSV curves of CoSe@NCNT/NCN after 2000 cycles (inset: i-t curve of 20h).

4. Conclusions

In summary, we have developed a simple and effective strategy to fabricate CoSe nanoparticles encapsulated

NCNT grafted onto NCN through a facile one-step pyrolysis method. The unique 3D hierarchical structure endows the CoSe@NCNT/NCN with large surface area, plentiful porosity and protects CoSe nanoparticles from harsh corrosive solution. The CoSe@NCNT/NCN exhibits remarkable electrochemical activity and favorable reaction kinetics for HER and OER, which is in comparison with the commercial Pt/C and IrO_2 catalyst, respectively. And the catalyst is better than most of previous reported carbon-based non-precious metal elecrocatalysts. The obtained catalyst may be regarded as a succedaneum of scarce noble metal catalysts for energy conversion systems with inexpensiveness, simple preparation and earth abundant advantages. This present work provides a new path for the design and synthesis of 3D transition metal dichalcogenide capped in N-doped carbon materials, which have outstanding catalytic performance and remarkable durability.

Conflicts of interest

The authors declare no conflict of interest

Author contributions

The manuscript was written through contributions of all authors. All authors have given approval to the final version of the manuscript. †These authors contributed equally.

Acknowledgements

This work is financially supported by the National Natural Science Foundation of China (No. 51602138).

Notes and references

[1] Y.-J. Yuan, Z.-T. Yu, D.-Q. Chen, Z.-G. Zou, Metal-complex chromophores for solar hydrogen generation, Chem. Soc. Rev., 46 (2017) 603-631.

[2] J. Wang, F. Xu, H. Jin, Y. Chen, Y. Wang, Non-Noble Metal-based Carbon Composites in Hydrogen Evolution Reaction: Fundamentals to Applications, Adv. Mater., 29 (2017) 1605838.

[3] K. Liu, H. Zhong, F. Meng, X. Zhang, J. Yan, Q. Jiang, Recent advances in metal–nitrogen–carbon catalysts for electrochemical water splitting, Materials Chemistry Frontiers, 1 (2017) 2155-2173.

[4] H. Jin, C. Guo, X. Liu, J. Liu, A. Vasileff, Y. Jiao, Y. Zheng, S.-Z. Qiao, Emerging Two-Dimensional Nanomaterials for Electrocatalysis, Chem. Rev., 118 (2018) 6337-6408.

[5] L. Han, S. Dong, E. Wang, Transition-Metal (Co, Ni, and Fe)-Based Electrocatalysts for the Water Oxidation Reaction, Advanced materials, 28 (2016) 9266-9291.

[6] Y. Yang, X. Liang, F. Li, S. Li, X. Li, S.P. Ng, C.L. Wu, R. Li, Encapsulating Co2 P@C Core-Shell Nanoparticles in a Porous Carbon Sandwich as Dual-Doped Electrocatalyst for Hydrogen Evolution, ChemSusChem, 11 (2018) 376-388.

[7] R. Jin, X. Li, Y. Sun, H. Shan, L. Fan, D. Li, X. Sun, Metal–Organic Frameworks-Derived Co2P@N-C@rGO with Dual Protection Layers for Improved Sodium Storage, ACS Applied Materials & Interfaces, 10 (2018) 14641-14648.

[8] K. Wu, Z. Chen, W.-C. Cheong, S. Liu, W. Zhu, X. Cao, K. Sun, Y. Lin, L. Zheng, W. Yan, Y. Pan, D. Wang, Q. Peng, C. Chen, Y. Li, Toward Bifunctional Overall Water Splitting Electrocatalyst: General Preparation of Transition Metal Phosphide Nanoparticles Decorated N-Doped Porous Carbon Spheres, ACS applied materials & interfaces, 10 (2018) 44201-44208.

[9] Y. Yang, K. Zhang, H. Lin, X. Li, H.C. Chan, L. Yang, Q. Gao, MoS2–Ni3S2 Heteronanorods as Efficient and Stable Bifunctional Electrocatalysts for Overall Water Splitting, ACS Catal., 7 (2017) 2357-2366.

[10] C. Zhang, B. Wang, J. Xiang, C. Su, C. Mu, F. Wen, Z. Liu, Microwave Absorption Properties of CoS2 Nanocrystals Embedded into Reduced Graphene Oxide, ACS applied materials & interfaces, 9 (2017) 28868-28875.

[11] Y. Zhang, A. Pan, L. Ding, Z. Zhou, Y. Wang, S. Niu, S. Liang, G. Cao, Nitrogen-Doped Yolk–Shell-Structured CoSe/C Dodecahedra for High-Performance Sodium Ion Batteries, ACS applied materials & interfaces, 9 (2017) 3624-3633.

[12] X. Zhao, H. Zhang, Y. Yan, J. Cao, X. Li, S. Zhou, Z. Peng, J. Zeng, Engineering the Electrical Conductivity of Lamellar Silver-Doped Cobalt(II) Selenide Nanobelts for Enhanced Oxygen Evolution, Angewandte Chemie, 56 (2017) 328-332.

[13] X. Wang, F. Li, W. Li, W. Gao, Y. Tang, R. Li, Hollow bimetallic cobalt-based selenide polyhedrons derived from metal–organic framework: an efficient bifunctional electrocatalyst for overall water splitting, Journal of Materials Chemistry A, 5 (2017) 17982-17989.

[14] P.R. Jothi, Y. Zhang, J.P. Scheifers, H. Park, B.P.T. Fokwa, Molybdenum diboride nanoparticles as a highly efficient electrocatalyst for the hydrogen evolution reaction, Sustainable Energy & Fuels, 1 (2017) 1928-1934.

[15] P.R. Jothi, Y. Zhang, K. Yubuta, D.B. Culver, M. Conley, B.P.T. Fokwa, Abundant Vanadium Diboride with Graphene-like Boron layers for Hydrogen Evolution, ACS Applied Energy Materials, 2 (2019) 176-181.

[16] H. Park, Y. Zhang, J.P. Scheifers, P.R. Jothi, A. Encinas, B.P.T. Fokwa, Graphene- and Phosphorene-like Boron Layers with Contrasting Activities in Highly Active Mo2B4 for Hydrogen Evolution, Journal of the American Chemical Society, 139 (2017) 12915-12918.

[17] P.R. Jothi, K. Yubuta, B.P.T. Fokwa, A Simple, General Synthetic Route toward Nanoscale Transition Metal Borides, Advanced materials, 30 (2018) e1704181.

[18] J.-T. Ren, L. Chen, C.-C. Weng, G.-G. Yuan, Z.-Y. Yuan, Well-Defined Mo2C Nanoparticles Embedded in Porous N-Doped Carbon Matrix for Highly Efficient Electrocatalytic Hydrogen Evolution, ACS applied materials & interfaces, 10 (2018) 33276-33286.

[19] S. Li, C. Cheng, A. Sagaltchik, P. Pachfule, C. Zhao, A. Thomas, Metal-Organic Precursor-Derived Mesoporous Carbon Spheres with Homogeneously Distributed Molybdenum Carbide/Nitride Nanoparticles for Efficient Hydrogen Evolution in Alkaline Media, Advanced Functional Materials, (2018) 1807419.

[20] R.S. Ryota Sakamoto, Keisuke Wada, Naoya Fukui, Hiroaki Maeda,, R.S. Joe Komeda, Koji Harano and Hiroshi Nishihara A pyrazine-incorporated graphdiyne nanofilm as a metal-free electrocatalyst for the hydrogen evolution reaction, J. Mater. Chem. A,, 6 (2018) 22189–22194.

[21] S. Li, Z. Yu, Y. Yang, Y. Liu, H. Zou, H. Yang, J. Jin, J. Ma, Nitrogen-doped truncated carbon nanotubes inserted into nitrogen-doped graphene nanosheets with a sandwich structure: a highly efficient metal-free catalyst for the HER, Journal of Materials Chemistry A, 5 (2017) 6405-6410.

[22] J. Wang, W. Cui, Q. Liu, Z. Xing, A.M. Asiri, X. Sun, Recent Progress in Cobalt-Based Heterogeneous Catalysts for Electrochemical Water Splitting, Advanced materials, 28 (2016) 215-230.

[23] W. Lu, R. Jiang, X. Yin, L. Wang, Porous N-doped-carbon coated CoSe2 anchored on carbon cloth as 3D photocathode for dye-sensitized solar cell with efficiency and stability outperforming Pt, Nano Research, 12 (2018) 159-163.

[24] Y. Huang, Z. Wang, Y. Jiang, S. Li, Z. Li, H. Zhang, F. Wu, M. Xie, L. Li, R. Chen, Hierarchical porous Co0.85Se@reduced graphene oxide ultrathin nanosheets with vacancy-enhanced kinetics as superior anodes for sodium-ion batteries, Nano Energy, 53 (2018) 524-535.

[25] M. Liao, G. Zeng, T. Luo, Z. Jin, Y. Wang, X. Kou, D. Xiao, Three-dimensional coral-like cobalt selenide as an advanced electrocatalyst for highly efficient oxygen evolution reaction, Electrochimica Acta, 194 (2016) 59-66.

[26] Y. Hou, S. Cui, Z. Wen, X. Guo, X. Feng, J. Chen, Strongly Coupled 3D Hybrids of N-doped Porous Carbon Nanosheet/CoNi Alloy-Encapsulated Carbon Nanotubes for Enhanced Electrocatalysis, Small, 11 (2015) 5940-5948.

[27] Z. Chen, R. Wu, Y. Liu, Y. Ha, Y. Guo, D. Sun, M. Liu, F. Fang, Ultrafine Co Nanoparticles Encapsulated in Carbon-Nanotubes-Grafted Graphene Sheets as Advanced Electrocatalysts for the Hydrogen Evolution Reaction, Adv. Mater., 30 (2018) 1802011.

[28] W. Zhou, J. Lu, K. Zhou, L. Yang, Y. Ke, Z. Tang, S. Chen, CoSe 2 nanoparticles embedded defective carbon nanotubes derived from MOFs as efficient electrocatalyst for hydrogen evolution reaction, Nano Energy, 28 (2016) 143-150.

[29] Y. Guo, P. Yuan, J. Zhang, H. Xia, F. Cheng, M. Zhou, J. Li, Y. Qiao, S. Mu, Q. Xu, Co_2P-CoN Double Active Centers Confined in N-Doped Carbon Nanotube: Heterostructural Engineering for Trifunctional Catalysis toward HER, ORR, OER, and Zn-Air Batteries Driven Water Splitting, Adv. Funct. Mater., 28 (2018) 1805641.

[30] N. Lu, T. Zhang, X. Yan, Y. Gu, H. Liu, Z. Xu, H. Xu, X. Li, Z. Zhang, M. Yang, Facile synthesis of 3D N-doped porous carbon nanosheets as highly active electrocatalysts toward the reduction of hydrogen peroxide, Nanoscale, 10 (2018) 14923-14930.

[31] G. Wang, Y. Deng, J. Yu, L. Zheng, L. Du, H. Song, S. Liao, From Chlorella to Nestlike Framework Constructed with Doped Carbon Nanotubes: A Biomass-Derived, High-Performance, Bifunctional Oxygen Reduction/Evolution Catalyst, ACS Appl Mater Interfaces, 9 (2017) 32168-32178.

[32] X.H. Li, S. Kurasch, U. Kaiser, M. Antonietti, Synthesis of monolayer-patched graphene from glucose, Angewandte Chemie, 51 (2012) 9689-9692.

[33] Y. Wang, X. Wang, M. Antonietti, Polymeric graphitic carbon nitride as a heterogeneous organocatalyst: from photochemistry to multipurpose catalysis to sustainable chemistry, Angewandte

Chemie, 51 (2012) 68-89.

[34] D. Das, K.K. Nanda, One-step, integrated fabrication of Co 2 P nanoparticles encapsulated N, P dual-doped CNTs for highly advanced total water splitting, Nano Energy, 30 (2016) 303-311.

[35] Z. Fan, J. Yan, L. Zhi, Q. Zhang, T. Wei, J. Feng, M. Zhang, W. Qian, F. Wei, A Three-Dimensional Carbon Nanotube/Graphene Sandwich and Its Application as Electrode in Supercapacitors, Adv. Mater., 22 (2010) 3723-3728.

[36] W. Yang, X. Liu, X. Yue, J. Jia, S. Guo, Bamboo-like carbon nanotube/Fe3C nanoparticle hybrids and their highly efficient catalysis for oxygen reduction, Journal of the American Chemical Society, 137 (2015) 1436-1439.

[37] L. Ma, R. Wang, Y.-H. Li, X.-F. Liu, Q.-Q. Zhang, X.-Y. Dong, S.-Q. Zang, Apically Co-nanoparticles-wrapped nitrogen-doped carbon nanotubes from a single-source MOF for efficient oxygen reduction, Journal of Materials Chemistry A, 6 (2018) 24071-24077.

[38] W. Wei, H. Liang, K. Parvez, X. Zhuang, X. Feng, K. Mullen, Nitrogen-doped carbon nanosheets with size-defined mesopores as highly efficient metal-free catalyst for the oxygen reduction reaction, Angew. Chem. Int. Ed. Engl., 126 (2014) 1596-1600.

[39] M. Yang, F. Feng, K. Wang, S. Li, X. Huang, L. Gong, L. Ma, R. Li, Synthesis of metal phosphide nanoparticles supported on Porous N-doped carbon derived from Spirulina for Universal pH value Hydrogen Evolution Reaction, ChemSusChem, 10.1002/cssc.201902920.

[40] Y. Zhou, R. Tian, H. Duan, K. Wang, Y. Guo, H. Li, H. Liu, CoSe/Co nanoparticles wrapped by in situ grown N-doped graphitic carbon nanosheets as anode material for advanced lithium ion batteries, Journal of Power Sources, 399 (2018) 223-230.

[41] K. Wang, Y. Chen, R. Tian, H. Li, Y. Zhou, H. Duan, H. Liu, Porous Co–C Core–Shell Nanocomposites Derived from Co-MOF-74 with Enhanced Electromagnetic Wave Absorption Performance, ACS applied materials & interfaces, 10 (2018) 11333-11342.

[42] Q. Dong, Q. Wang, Z. Dai, H. Qiu, X. Dong, MOF-Derived Zn-Doped CoSe2 as an Efficient and Stable Free-Standing Catalyst for Oxygen Evolution Reaction, ACS applied materials & interfaces, 8 (2016) 26902-26907.

[43] D. Kong, H. Wang, Z. Lu, Y. Cui, CoSe2 Nanoparticles Grown on Carbon Fiber Paper: An Efficient and Stable Electrocatalyst for Hydrogen Evolution Reaction, J. Am. Chem. Soc., 136 (2014) 4897-4900.

[44] H. Wang, X. Wang, D. Yang, B. Zheng, Y. Chen, Co0.85Se hollow nanospheres anchored on N-doped graphene nanosheets as highly efficient, nonprecious electrocatalyst for hydrogen evolution reaction in both acid and alkaline media, Journal of Power Sources, 400 (2018) 232-241.

[45] C.-Z. Yuan, Y.-F. Jiang, Z. Wang, X. Xie, Z.-K. Yang, A.B. Yousaf, A.-W. Xu, Cobalt phosphate nanoparticles decorated with nitrogen-doped carbon layers as highly active and stable electrocatalysts for the oxygen evolution reaction, Journal of Materials Chemistry A, 4 (2016) 8155-8160.

[46] L. Liu, S. Zhang, F. Yan, C. Li, C. Zhu, X. Zhang, Y. Chen, Three-Dimensional Hierarchical MoS2 Nanosheets/Ultralong N-Doped Carbon Nanotubes as High-Performance Electromagnetic Wave Absorbing Material, ACS Appl Mater Interfaces, 10 (2018) 14108-14115.

[47] K. Wang, W. Gao, P. Jiang, K. Lan, M. Yang, X. Huang, L. Ma, F. Niu, R. Li, Bi-functional catalyst of porous N-doped carbon with bimetallic FeCu for solvent-free resultant imines and hydrogenation of nitroarenes, Molecular Catalysis, 465 (2019) 43-53.

[48] J. Yang, H. Gao, S. Men, Z. Shi, Z. Lin, X. Kang, S. Chen, CoSe2 Nanoparticles Encapsulated by N-Doped Carbon Framework Intertwined with Carbon Nanotubes: High-Performance Dual-Role Anode

Materials for Both Li- and Na-Ion Batteries, Adv Sci (Weinh), 5 (2018) 1800763.

[49] J. Durst, A. Siebel, C. Simon, F. Hasché, J. Herranz, H.A. Gasteiger, New insights into the electrochemical hydrogen oxidation and evolution reaction mechanism, Energy Environ. Sci., 7 (2014) 2255-2260.

[50] H. Osgood, S.V. Devaguptapu, H. Xu, J. Cho, G. Wu, Transition metal (Fe, Co, Ni, and Mn) oxides for oxygen reduction and evolution bifunctional catalysts in alkaline media, Nano Today, 11 (2016) 601-625.

[51] S. Wang, J. Qin, T. Meng, M. Cao, Metal–organic framework-induced construction of actiniae-like carbon nanotube assembly as advanced multifunctional electrocatalysts for overall water splitting and Zn-air batteries, Nano Energy, 39 (2017) 626-638.

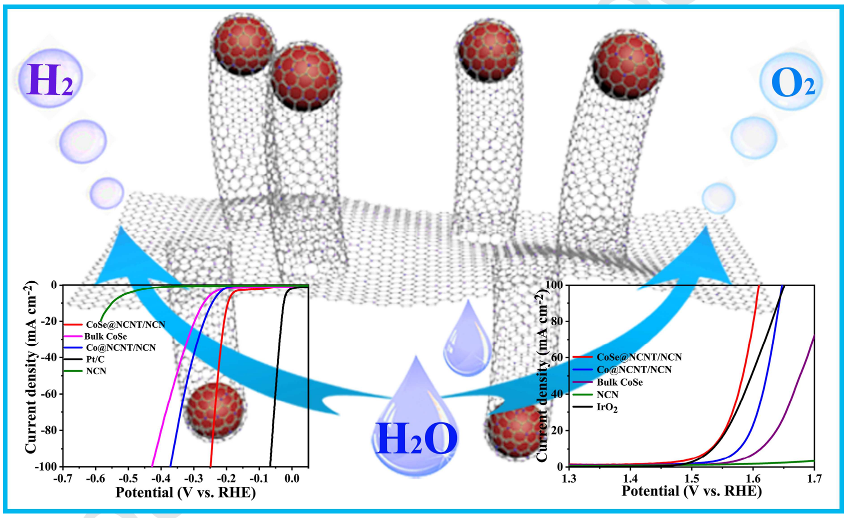

The manuscript was written through contributions of all authors. All authors have given approval to the final version of the manuscript.

The authors declare no conflict of interest